CHEMISTRY

Designing self-propelled, chemically active sheets: Wrappers, flappers, and creepers

Abhrajit Laskar, Oleg E. Shklyaev, Anna C. Balazs*

Catalyst-coated, hard particles can spontaneously generate fluid flows, which, in turn, propel the particles through the fluid. If the catalyst-coated object were a deformable sheet, then the self-generated flows could affect not only the sheet's motion but also its shape. By developing models that capture the interrelated chemical, hydrodynamic, and mechanical interactions, we uncover novel behavior emerging from the previously unstudied coupling between active, soft sheets and the surrounding fluid. The chemically generated flows "sculpt" the sheet into various forms that yield different functionalities, which can be tailored by modifying the sheet's geometry, patterning the sheet's surface with different catalysts, and using cascades of chemical reactions. These studies reveal how to achieve both spatial and temporal controls over the position and shape of active sheets and thus use the layers to autonomously and controllably trap soft objects, perform logic operations, and execute multistage processes in fluid-filled microchambers.

INTRODUCTION

Chemically active, catalytic objects in aqueous environments can autonomously perform a variety of vital functions (*1*, *2*). The capabilities and functionalities of these active objects are determined by the specific way they couple to the fluidic environment. The simplest of such objects is a patch of catalysts that is immobilized on the surface of a fluid-filled microchannel (*3*). In the presence of the appropriate reactants, the stationary catalytic patch can act as a "chemical pump," generating density gradients that drive fluid flows, which, in turn, transport chemicals and immersed particles (*4*). The flows generated by the chemical pumps, however, do not affect the location or shape of the pump. Mobile chemical pumps such as catalyst-coated nano- and microscopic particles (i.e., chemical "motors") can undergo self-propelled motion (*1*, *2*) and thus autonomously repair broken electrical circuits (*5*) or act as active drug delivery systems (*6*, *7*). In the case of chemical motors, the motion of the active particles affects the fluid flow, and the flow, in turn, affects the position of the particles (*8*). The fluid does not, however, alter the shape of the particle. Catalyst-coated, flexible sheets would constitute the next level of complexity because they introduce additional degrees of freedom. The chemically active sheets could generate fluid flows that propel this object through the solution; now, however, the generated flows would affect not only the position of the sheet but also the shape of this object. Such reconfigurable, self-propelled objects would greatly expand the utility of fluidic devices, allowing them to perform self-sustained operations that were previously unattainable with stationary chemical pumps or active hard particles. To date, however, there have been no theoretical or experimental studies on chemically active, flexible sheets programmed to perform mechanical work within the surrounding fluid. Such studies are needed to design flexible, small-scale machines that convert chemical energy into spontaneous structural reconfiguration and movement and thus enable fluidic devices to carry out a whole new repertoire of useful tasks.

Herein, we develop a model for microscopic, catalyst-coated elastic sheets and show that the chemically generated flows around the sheet "sculpt" this layer into various forms that can provide different functionalities. This functionality can be tailored by modifying the sheet's initial shape, flexibility, the arrangement of different catalysts on the sheet, and the palette of chemicals interacting with the sheet. We also demonstrate how the catalytic reactions can be harnessed to coordinate the spatiotemporal behavior of the fluid flows within the container and thus achieve greater control of the sheet's shape and dynamic behavior. As shown below, these studies reveal conditions where the active sheets controllably bend to grasp particulates in solution, perform simple logic operations in a microfluidic device, and undergo novel forms of self-propelled locomotion (tumbling or creeping) along a surface. In all these cases, the soft sheets change shape and thus respond mechanically to the generated flows. Materials exhibiting mechanical responses to stimuli are particularly important for designing soft robotics systems and, more generally, improving our understanding of systems that can undergo self-sustained actuation and locomotion (*9*).

As detailed in the following section, the active sheets in our model are described as a network of interconnected nodes. The restoring force between the nodes drives them to act as a coherent fabric, where deformations in one portion of the material will affect the entire system. In this sense, the cooperative interactions in an elastic, active sheet can extend over larger length scales than the collective dynamics of a comparable number of individual particles (i.e., that are not physically bound into a network but are simply coupled by hydrodynamic interactions). Notably, a variety of synthetic methods could be used to fabricate such active sheets, including approaches that involve cross-linking catalytically active particles (*10*) or anchoring catalysts onto polymeric layers.

RESULTS

Theoretical modeling

For the chemically active objects to perform mechanical work in the host solution, the chemical reactions occurring at the object must be coupled to the motion of the surrounding fluid. One particularly effective means of achieving this coupling is through the mechanism of solutal buoyancy (*11*, *12*), which can be realized by coating the object with a catalyst and immersing it into a solution of appropriate reactants. The catalytic coating decomposes dissolved reactants into the products of the chemical reaction. The resulting spatial distribution of the reactants and products introduces the density variations that drive

Department of Chemical Engineering, University of Pittsburgh, Pittsburgh, PA 15260, USA.
*Corresponding author. Email: balazs@pitt.edu

the spontaneous motion of the fluid, which thereby imposes a fluid drag on the objects in the solution. Since total mass is conserved during the reaction, the change in density that occurs when reactants are converted to products arises because the product molecules occupy a different volume in solution compared to the reactants (*11*). Thus, there is a slight expansion or contraction of the fluid. This microscopic effect is characterized by the coefficients of expansion (β), which are specific to the particular chemicals participating in a given reaction. [These density variations are analogous to those due to thermal buoyancy (*12*), where variations in heat produce the density gradients that produce flow.]

In a confined chamber, the solutal buoyancy mechanism will produce circular convective motion (due to the continuity of the fluid) (*3*, *11*, *12*). Namely, if the products of the chemical reaction are denser than the reactants, then the product-rich fluid flows downward to the bottom of the channel, and its volume is replaced by the reactant-rich fluid. Conversely, if the products are less dense than the reactants, then the fluid will rise upward and its position is replaced by fresh, reactant-rich solution.

In our model, the solutal buoyancy force is given by $\mathbf{F}_b = \mathbf{g}\rho_0\Sigma\beta_i C_i$, which depends on gravity $\mathbf{g}$, solvent density ρ_0, the concentrations of each dissolved chemical C_i, and the corresponding expansion coefficients β_i (*11*, *12*). This buoyancy force drives the fluid motion that, in turn, affects the configuration of the catalyst-coated sheet. The continuous, flexible sheet is discretized into a network of N chemically active nodes characterized by positions $\mathbf{r}_k$ (with $1 \le k \le N$) that are interconnected by elastic bonds (see Fig. 1A), which can stretch and bend. Hence, the governing equations that describe the entire system are as follows: the continuity and Navier-Stokes [in the Boussinesq approximation (*13*)] equations for the fluid dynamics; the equation for the advection, diffusion, and reaction of the dissolved chemical species; and the equation for the dynamic behavior of the nodes of the sheet. The respective equations are given below

$$\nabla\cdot\mathbf{u} = 0 \tag{1}$$

$$\frac{\partial\mathbf{u}}{\partial t} + (\mathbf{u}\cdot\nabla)\mathbf{u} = -\frac{1}{\rho_0}\nabla p + \nu\nabla^2\mathbf{u} + \frac{1}{\rho_0}(\mathbf{F}_b + \mathbf{F}_{el}) \tag{2}$$

$$\frac{\partial C_i}{\partial t} + (\mathbf{u}\cdot\nabla)C_i = D_i\nabla^2 C_i - SK_d\sum_{k=1}^{N}\delta(\mathbf{r}_k - \mathbf{r}) \tag{3}$$

$$\frac{\partial\mathbf{r}_k}{\partial t} = \mathbf{u} + \mu\left(\mathbf{F}_g + \sum_{j=1}^{6}\mathbf{F}^{n-w}(\mathbf{r}_k - \mathbf{r}_k^{W_j}) + \sum_{k\neq l}\mathbf{F}^{n-n}(\mathbf{r}_l - \mathbf{r}_k) + \mathbf{F}_{el}(\mathbf{r}_k)\right), \quad 1\le k, l\le N \tag{4}$$

Here, ∇ is the spatial gradient operator and ν is the kinematic viscosity of water. The local fluid velocity and pressure are given by $\mathbf{u}$ and p, respectively.

Unless stated otherwise, we impose no-slip boundary conditions ($\mathbf{u} = 0$) at the solid walls of the container. For the reagent C_i, we use three different boundary conditions to describe different surface properties of the container walls. In particular, we consider the following scenarios: (i) when the wall is coated with enzyme, (ii) no chemical penetration through the boundaries, and (iii) when the reagent is released into the chamber. The respective conditions for the container boundary, with surface normal $\hat{n}$, are expressed as

$$-D_i\frac{\partial C_i}{\partial n} = \begin{cases} \dfrac{r^{e}_{m,wall}C_i}{K_M + C_i}, & \text{(i)enzyme-coated wall} \\ 0, & \text{(ii)no flux} \\ R(t), & \text{(iii)chemical influx} \end{cases} \tag{5}$$

As described by Eq. 3, the ith reagent of concentration C_i diffuses with the diffusion constant D_i and is advected by the flowing fluid, which is moving with a velocity $\mathbf{u}$. The reactant is consumed in the presence of the catalytic sheet at the positions $\mathbf{r}_k$ of the constituent nodes with a reaction rate given by SK_d, where K_d is the reaction rate per unit area and S is the surface area per node of the sheet. The catalytic reactions occurring at the surface of the sheet are modeled using the Michaelis-Menten reaction rates

$$K_d = \frac{r^{e}_{m,sheet}C_i}{K_M + C_i} \tag{6}$$

Here, the maximal reaction rate $r^{e}_{m,sheet} = k_e[E]$ incorporates the reaction rate per molecule of enzyme k_e and the areal enzyme concentration $[E]$, and K_M is the Michaelis constant. As described below, we also tailor the maximal reaction rate on the inner walls of the chamber, to control the sequences of spatial and temporal events. (Generally, the reaction rate K_d also encompasses information about the stoichiometry of the reaction to ensure the conservation of mass during the reaction. In all the chemical reactions considered below, 1 mol of the reactant is converted exactly to 1 mol of the product, and therefore, such corrections to K_d are not required.)

Equation 4 describes the dynamics of each constituent node of the sheet; the elastic forces, $\mathbf{F}_{el}$, that arise due to the stretching and bending of bonds connecting the nodes are governed by the linear constitutive relations for a Kirchoff rod (*14*). The minimum elastic energy is attained when the sheet is in the flat configuration. To model the excluded volume of the sheet, each node also experiences a steric repulsion with the other nodes in the sheet and with the confining walls. Given that $\mathbf{r}_k - \mathbf{r}_k^{W_j}$ specifies the vector from a constituent node k to the closest point on the wall labeled as W_j, then $\mathbf{F}^{n-w}(\mathbf{r}) = -\frac{\partial U(r)}{\partial\mathbf{r}}$ is the node-wall repulsive force, which is modeled using the Morse potential

$$U(r) = \begin{cases} \varepsilon(1 - \exp[-\omega(r - r_0)])^2, r < r_0 \\ 0, \quad r \ge r_0 \end{cases} \tag{7}$$

The parameters ε and ω denote the strength and width of the potential, respectively, and r_0 is the equilibrium (and cutoff) distance of the potential. The steric repulsion between nodes l and k is described by $\mathbf{F}^{n-n}(\mathbf{r}_l - \mathbf{r}_k)$, which has the same functional form of the potential as Eq. 7.

The density of the sheet (ρ_s) is greater than the density of the pure solution (ρ_0), and thus, the sheet undergoes sedimentation. Consequently, all the nodes in the sheet experience an additional external force, $\mathbf{F}_g = V(\rho_s - \rho_0)\mathbf{g}$. Here, V is the effective volume of each node, defined as the volume of the sheet divided by the number of nodes. At the bottom wall of the container, the sedimentation force due to gravity is counteracted by the steric repulsion between the nodes of the sheet and the wall (as modeled through forces $\mathbf{F}^{n-w}$). For some

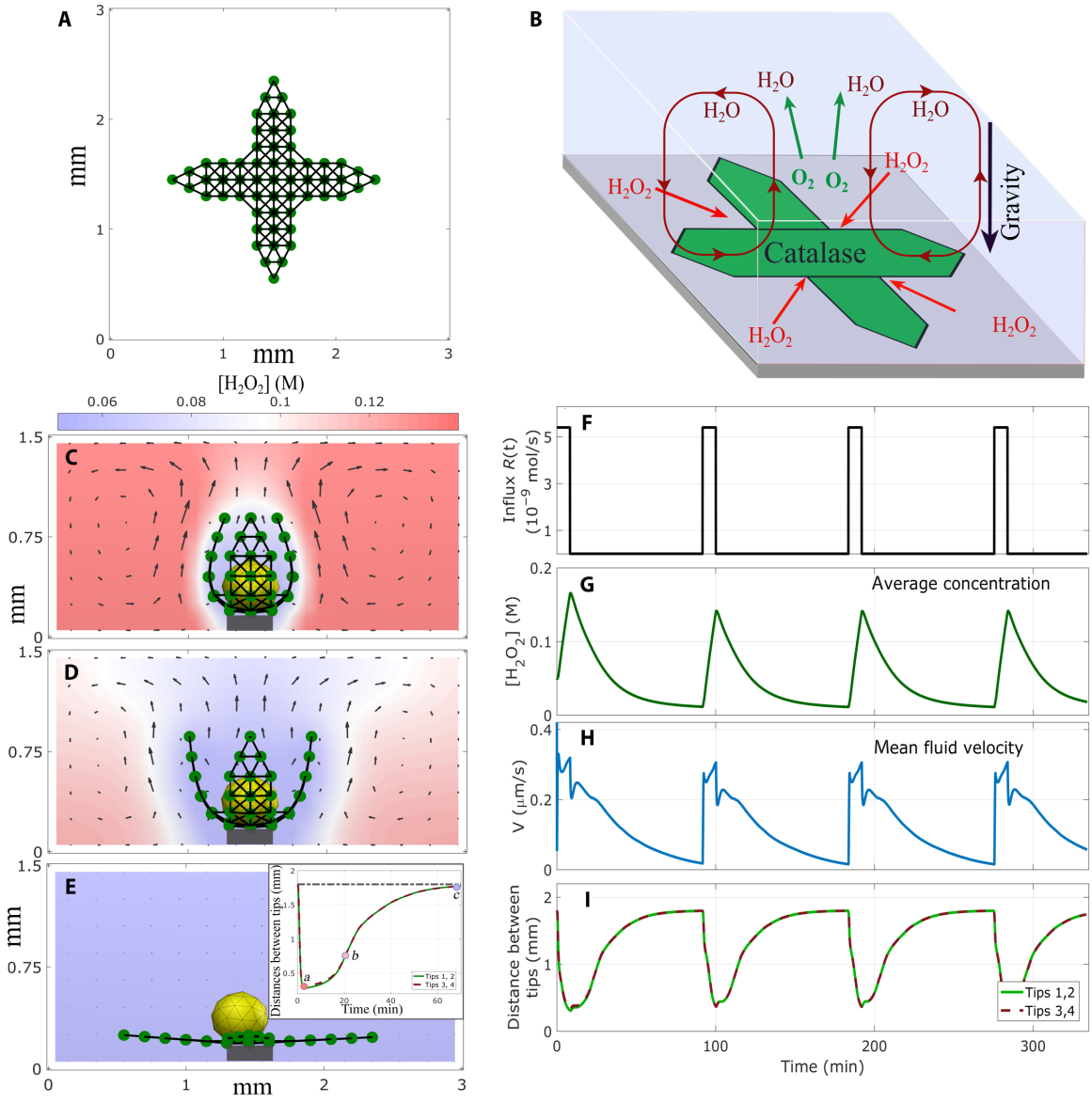

Fig. 1. Chemomechanical response of catalse-coated sheet. (**A**) Top-down view of a fluidic chamber containing a catalase-coated flower-like, elastic sheet composed of nodes (indicated by green dots) and connected by bonds (black lines) and (**B**) schematic of the solutal convection due to the catalytic reaction on the sheet. (**C** to **E**) Sequential wrapping and unwrapping of a passive sphere (in yellow) by a catalase-coated sheet ($r^{cat}_{m,sheet} = 6.5 \times 10^{-4}$ mol m^{-2} s^{-1}), positioned in parallel to the bottom surface at a distance $h = 0.19$ mm. Catalase decomposes hydrogen peroxide to less dense products, oxygen and water, which rise upward to produce an inward convective flow at the bottom of the microchamber. Black arrows indicate the directionality and magnitude of the flow field, and the color bar indicates the concentration of H_2O_2 in the solution. Inset in (E): Relative distances between the tips of opposite pairs of petals. As H_2O_2 is consumed, the convective flow is diminished and the sheet gradually opens up to return to the flat state. (**F** to **I**) Repetitive wrapping and unwrapping of petals with regular influxes of hydrogen peroxide. (F) H_2O_2 introduced periodically through the side walls at a rate $R = 5.4 \times 10^{-9}$ mol s^{-1}. (G) Concentration of the reactant decreases as it is decomposed into products, only to increase with the next input of H_2O_2. (H) Mean velocity reaches a maximum with each influx of H_2O_2. (Average is taken over the velocities in the central, vertical plane that cuts through the center of the decorative sphere.) (I) Distance between the tips of respective pairs of petals, showing the periodic opening and closing.

applications, we fix the center of the elastic sheet horizontally at a distance h above the bottom wall.

Before detailing the quantitative results obtained from the simulations, we first provide a qualitative description of how the above parameters regulate the behavior of the system. In particular, there are three independent groups of parameters that control the respective behavior of the three main components of the system: (i) the chemical composition of the solution, (ii) the fluid dynamics, and (iii) the elastic sheet. The parameters characterizing the spatially and temporary varying solution include the chemical concentrations C_i, diffusivities D_i, and the reaction rates $\frac{k_e[E]C_i}{K_M+C_i} S$. The latter reaction rates describe the production (and consumption) of the chemicals at the enzyme-coated boundaries. The parameters ν and ρ describe the dynamic properties of the fluid. The parameters characterizing the mechanical properties of the sheet are given by the elastic coefficients describing the Kirchhoff rods (*14*); these parameters detail the nature of the connection between

the discretized sheet nodes and define the sheet flexibility. In addition, the distance h between the sheet and the bottom wall determines how efficiently the sheet "catches" the fluid flow, which decreases to zero at the wall (due to no-slip boundary conditions).

The production (consumption) of the chemicals is controlled by the area of the enzyme-coated surface, S; the magnitude of the turnover rate k_e of each enzyme molecule; and the areal concentration of the molecules, $[E]$. Increasing any of these parameters increases the production (consumption) of the chemicals in the chamber. The spatially and temporarily nonuniform chemical composition of the solution gives rise to the solutal buoyancy forces that drive fluid motion.

If we consider the linear response regime (slow flows), then the fluid velocities are proportional to the ratio between the buoyancy force $\rho_0 g\beta\Delta C L^3$, moving the solution within a volume L^3, and the viscous force $\nu^2\rho_0$, resisting the motion. This ratio is described by the Grashof number, $\frac{g C\beta\Delta C L^3}{\nu^2}$, which indicates that the flow velocities can be increased by either using chemicals with higher solutal expansion coefficients $\beta = \frac{\partial\rho}{\partial C}$, imposing larger chemical gradients ∇C across the domain, or increasing the characteristic length L of the system.

For a given flow field, the elastic parameters describing the sheet can be adjusted to optimize the range of the sheet's motion for a particular application. For the flower-like design, the distance h between the bottom wall and the sheet controls the amount of the fluid drag experienced by the sheet. Thinner sheets that lie closer to the bottom wall experience a smaller fluid drag. Alternatively, for a given set of parameters characterizing the sheet and chosen offset distance h, the chamber geometry and the types of the reactants and enzymes can be chosen to optimize the desired functionality of the system.

Notably, in our formulation, there is no direct coupling between the dynamics of the chemicals and the mechanical properties of the sheet. The effect of the chemical reaction on the configuration of the sheet is mediated by the generated fluid flows.

Our approach for solving the governing equations (Eqs. 1 to 4) in the presence of the specified boundary conditions (Eq. 5) is detailed in Methods. Below, we describe different scenarios that illustrate the distinctive behavior that is achievable with active sheets, including samples that act as "wrappers," "flappers," and "creepers."

Designing active sheets

For the enzymatic chemical reactions considered here, solutal buoyancy is the dominant mechanism that gives rise to the fluid flow (*11*, *12*). While a number of different chemical reactions can produce such solutal buoyancy effects, below, we select specific reactions to demonstrate proof of principle. As a first example, we choose aqueous solutions containing hydrogen peroxide (H_2O_2), which is decomposed into water (H_2O) and oxygen (O_2) in the presence of the enzyme catalase

$$H_2O_2 \xrightarrow{\text{catalase}} H_2O + O_2 \tag{8}$$

For the above reaction, we set $r^{\text{cat}}_{\text{m,sheet}} = 6.5 \times 10^{-4}$ mol m^{-2} s^{-1} and $K_M = 0.093$ M for both faces of the sheet; these values are consistent with known experimental values for catalase (*15*, *16*).

We exploit this buoyancy mechanism to design flexible, active sheets that adopt geometrical configurations appropriate for performing different functions. To demonstrate the versatility of our approach, we first consider a flower-like, catalase-coated sheet (Fig. 1A) located at a distance of $h = 0.19$ mm from the bottom of a fluid-filled microchamber. The schematic in Fig. 1B illustrates the flow field that can be generated by a catalyst-coated flat sheet placed parallel to the bottom surface. In the following examples, the center of the flower is attached to the bottom wall, and the four petals are free to bend about this core. This petal arrangement provides a simple yet effective geometry for binding and wrapping an object in the solution (e.g., the sphere in Fig. 1, C and D).

Initially, the elastically relaxed petals stay parallel to the bottom wall and H_2O_2 is then uniformly dispersed in the chamber. The catalase decomposes H_2O_2 to less dense products (H_2O and O_2), which generate an inward flow, where the product-rich fluid rises upward and the reactant-rich fluid flows toward the sheet along the bottom wall. As indicated by the calculated velocity profiles (black arrows in Fig. 1C), this inward flow drags the elastic petals into an upward configuration, away from the wall. The petals' upward movement is reinforced by the circulating flow under the sheet (arising from the continuity of the confined fluid). To quantify the amplitude of the petal motion, we measure the separation distance between the tips of opposing petals as a function of time (inset in Fig. 1E). The plot indicates that this distance approaches zero as the flower closes its petals.

To visualize the petals' wrapping capabilities, we introduced an uncoated, passive sphere that is placed at the center of the flower and held at this position by gravity (Fig. 1, C to E). [The sphere is constructed using the immersed boundary (IB) method (*14*), as described in Methods.] As can be seen, the petals effectively envelop this central sphere. In this capacity, the petals can grasp and trap microscopic particulates or biological cells in solution. Because the sheet is soft and deformable, these aquatic wrappers might not affect the viability of samples and could thus facilitate biological assays on living microorganisms in microfluidic devices.

Ultimately, all the reactants for the system in Fig. 1C are consumed and the flow ceases to circulate. To release the elastic stresses within the deformed sheet, the petals now open up and expose the decorative sphere (Fig. 1D). The separation distance between the opposing tips of the petals returns to that in the initial, flat configuration (Fig. 1E). The petals can, however, be made to retain their closed structure for a specified amount of time by replenishing the solution with fresh reactants. Moreover, the petals can be made to open and close periodically if H_2O_2 is introduced [prescribed by the fluxes, $R(t)$ through the side walls as given by Eq. (5, iii)] at regular time intervals, as indicated in Fig. 1F. The concentration of the reactant decreases as it is decomposed into products, only to increase with the next input of H_2O_2 (Fig. 1G). The periodic increases in the reactant lead to regular spikes (Fig. 1H) in the average velocity of the fluid (which was obtained as the average of the velocities in the central, vertical plane that cuts through the center of the decorative sphere). Figure 1I shows that the closest approach of the opposing petals occurs at the maximum of the fluid velocity.

This rhythmic wrapping and unwrapping can be achieved with other couplings of catalyst-coated petals and the appropriate reagents in solution. For example, in the presence of the enzyme glucose oxidase (GOx), the reactants D-glucose and O_2 are transformed into gluconic acid and H_2O_2 (Eq. 9)

$$\text{D-glucose} + O_2 \xrightarrow{\text{GOx}} \text{gluconic acid} + H_2O_2 \tag{9}$$

Because the products are lighter than the reactants, this system also gives rise to an inward flow around the four petals and behaves in a manner similar to that in Fig. 1 (C to I).

The dynamic behavior and coordination among the individual petals can be tailored further by coating the petals with different catalysts and introducing a cascade of chemical reactions, where the product of one catalytic reaction is the reactant for the second. The reactions described above form an ideal coupling because the H_2O_2 produced by the reaction in Eq. 9 is the reactant for the reaction in Eq. 8. Figure 2 (A and B) shows the temporal behavior of a four-petal structure, where two of the opposing petals are coated with catalase (in green), and the remaining two petals are coated with GOx (in pink).

To activate the system in Fig. 2, D-glucose and O_2 are initially uniformly dispersed in the solution. GOx transforms these reactants into lighter products (Eq. 9). The resulting upward flow drives the pink petals to fold and join together (Fig. 2A). The decrease and ultimate consumption of the reactants in Eq. 9 stop the flow of fluid around the pinks petals and cause them to unfold to their original, flat position (Fig. 2B) parallel to the bottom wall. The concomitant increase in H_2O_2 (Fig. 2C) promotes the reaction in Eq. 8 and drives the flow field to bend the green petals upward and move toward each other (see Fig. 2B). As H_2O_2 is decomposed, the green petals will assume their initial flat configuration (Fig. 2D) parallel to the bottom wall.

The temporal delay in the folding of the pink and the green petals is clear in Fig. 2 (A and B), where one set of petals is folded, while the other remains flat and parallel to the bottom surface. This temporal behavior can also be seen in Fig. 2D, which shows the coordinates of the opposing pairs as a function of time; the minima of the curves correspond to the folded state of the petals, and it is clear that these minima are shifted in time.

In harnessing a cascade of chemical reactions to perform mechanical work, the rates of the different reactions should be coordinated to achieve the desired time-dependent behavior. The rates of the reactions

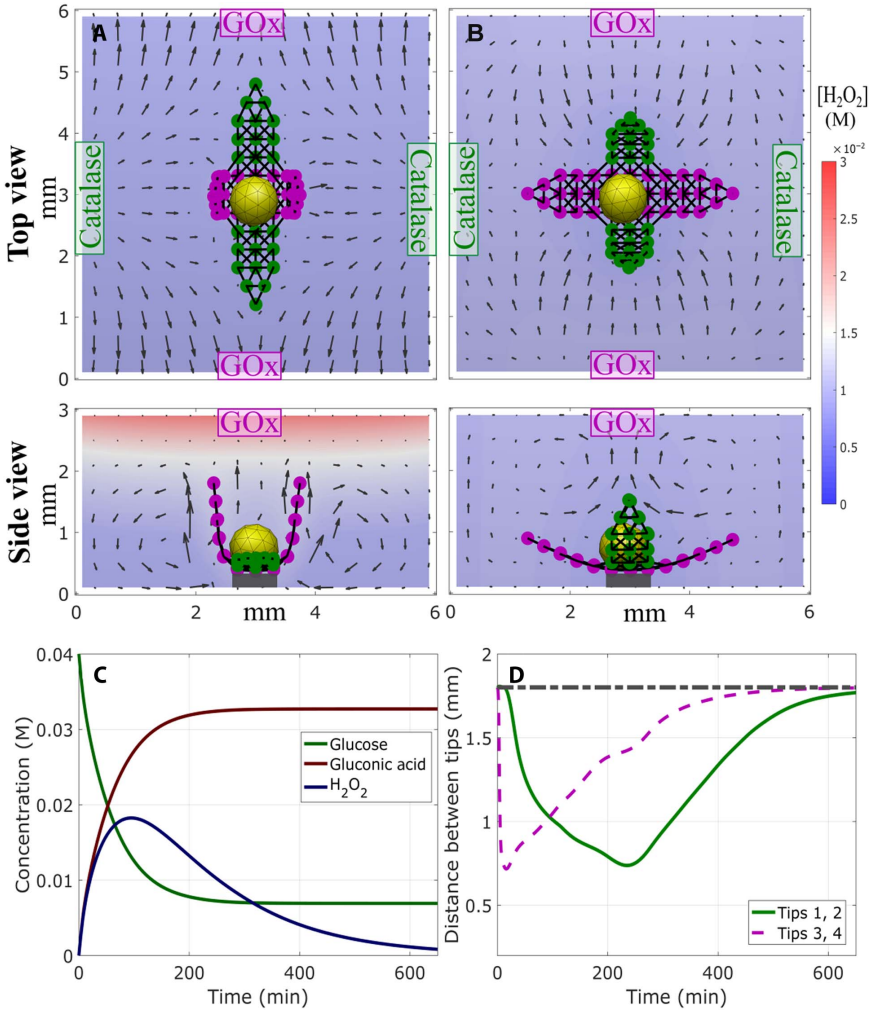

Fig. 2. Top and side views of the bending and unbending of the respective catalase-coated (green) and GOx-coated (pink) petals. Coordinated behavior of the petals involves the reaction cascade in Eqs. 8 and 9. (**A**) Inward flow generated by the decomposition of D-glucose and O_2 drives the pink petals to fold and join together. (**B**) With the consumption of these reactants, the pink petals unfold and the concentration of H_2O_2 increases in the medium. The decomposition of H_2O_2 on the green petals drives an inward flow that causes the bending of the green petals. (**C**) Temporal variation of concentrations of chemicals participating in the reaction cascade given by Eqs. 8 and 9. As expected, the concentration of hydrogen peroxide [the product of the first reaction (Eq. 9) and the reactant for the second reaction (Eq. 8)] initially increases and then decreases. (**D**) Temporal delay between the folding of the pairs of catalase- and GOx-coated petals is characterized by the difference in time between the minima of the plots. To obtain an appreciable time delay in the relative dynamic behavior of the green and pink petals, we specified the following areal concentrations of the enzymes on the petals and chamber walls: $r^{cat}_{m,petal} = 2.7 \times 10^{-4} mol\,m^{-2}s^{-1}$, $r^{gox}_{m,petal} = 2.7 \times 10^{-5} mol\,m^{-2}s^{-1}$, $r^{cat}_{m,sidewall} = 1.2 \times 10^{-5} mol\,m^{-2}s^{-1}$, $r^{gox}_{m,sidewall} = 6.7 \times 10^{-6} mol\,m^{-2}s^{-1}$, and $r^{gox}_{m,topwall} = 2.7 \times 10^{-5} mol\,m^{-2}s^{-1}$.

are characterized by the product $r^{e}_{m,petal}S$ (in moles per second), where $r^{e}_{m,petal}$ is the maximal reaction rate and S is the surface area of a catalytic site (e.g., the size of a node in our simulations). Notably, the maximal rate of reaction for the GOx-catalyzed reaction ($r^{gox}_{m,petal} = 2.7 \times 10^{-5}$ mol m^{-2} s^{-1}) is significantly slower than the one catalyzed by catalase ($r^{cat}_{m,petal} = 2.7 \times 10^{-4}$ mol m^{-2} s^{-1}) (*15*–*17*). There are two distinct ways we can increase the rate of transformation of glucose into H_2O_2 (Eq. 9) and thereby coordinate the reactions in Eqs. 8 and 9. First, we can pattern the space by coating the walls of the container with catalyst and thus tailor the surface area S to increase the rate of reaction. Second, we can tune the time scales for the different reactions by adjusting $r^{e}_{m,pos} = k_e[E]$, which can readily be altered by changing $[E]$, the areal concentration of catalyst on the surface. Because the petals are driven by fluid patterns appropriately organized in both space and time, we achieve the sequential behavior presented in Fig. 2.

In the example in Fig. 2, we coat the top walls of the container with GOx ($r^{gox}_{m,topwall} = 2.7 \times 10^{-5}$ mol m^{-2} s^{-1}). In addition, we coat the side walls opposite to the GOx-coated petals with catalase and coat the side walls opposite to the catalase-coated petals with GOx. The areal concentrations of enzymes $[E]$ and hence the corresponding reaction rates at the GOx-coated and catalase-coated walls are adjusted to maximize the time delay between the sequential wrappings by the different types of petals. Moreover, the concentrations of the enzyme are greater on the individual petals $r^{e}_{m,petal}$ than on the respective walls $r^{e}_{m,sidewall}$ (the corresponding specific values of $r^{e}_{m,sidewall} = k_e[E]$ are given in the caption for Fig. 2) and hence the rate of reaction is greater at the petals than at the walls.

This spatial arrangement of the two different enzymes on the container walls ensures that one set of petals (e.g., pink) remains localized on the bottom wall as the opposing petals (green) rise up and join together. The schematic in Fig. 3 illustrates how the combined flow fields act to regulate the petals in this manner. Namely, H_2O_2 generated in Eq. 9 reacts not only with the catalase-coated petals but also with the catalase-coated side walls (facing the GOx petals). The high reaction rate on the catalase petals causes the enzyme to rapidly decompose H_2O_2 and thereby generate an inward flow (toward the flower at the bottom) that pushes the green petals upward. Concomitantly, the slower reaction on the catalase-coated side wall (due to lower enzyme concentration) produces an outward flow (away from the flower and toward the walls)

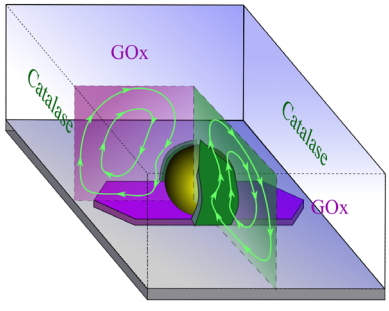

Fig. 3. Schematic describing temporal regulation of petals. To achieve the temporal delay between the closing of the opposing petals, the side walls adjacent to GOx-coated petals are coated with catalase, and the side walls adjacent to catalase-coated petals are coated with GOx. Consumption of H_2O_2 happens not only on catalase-coated green petals but also on the appropriate side walls. Consumption of H_2O_2 at these side walls creates an outward flow along GOx-coated pink petals that speeds up the movement of these petals to the horizontally flat state.

in the vertical plane perpendicular to the pink petals (see Fig. 3). This flow field affectively pushes the pink petals down onto the bottom wall. Since the reaction rate is lower at the catalase-coated side walls than at the catalase-coated petals, the decomposition of H_2O_2 is slower at the wall and ensures that the flow directed to the side walls holds the pink petals open while the green petals remain upright.

Similarly, coating the opposite petals and perpendicular side walls with GOx generates flow patterns that promote the upward folding of the GOx-coated petals while pushing catalase-coated petals to the bottom. In other words, the flow patterns generated at the appropriate pairs of side walls and around the petals guarantee that the folding of the different pairs of petals is separated in time.

In the above example, we exploited the two catalytic processes in a reaction cascade to achieve temporal control over quasi–two-dimensional objects. The independent opening and closing of the different petals allow them to be used as "gates" that regulate the motion of particles within the chamber and thereby allow the device to autonomously perform multistage processes. Instead of using the reaction cascade involving Eqs. 8 and 9, we now use two independent catalytic reactions and take advantage of the specificity of the catalysts to the respective reactants to enable these physical gates to act as chemical logic gates, or flappers.

In addition to Eq. 8, we now use the following chemistry

$$\text{PNPP} \xrightarrow{\text{acid phosphatase}} \text{PNP} + \text{NaH}_2\text{PO}_4 \qquad (10)$$

where the enzyme acid phosphatase (AP) decomposes *p*-nitrophenylphosphate hexahydrate (PNPP) into *p*-nitrophenol (PNP) and monosodium phosphate (NaH_2PO_4). Again, the products are lighter than the PNPP reactant. The geometry of the system in Fig. 4 is the same as that in the previous cases, but now, two opposing "flaps" are covered with AP (the yellow petals) and catalase (the green petals). Just as in the above scenario, the opposing walls are coated with the appropriate catalyst (see Fig. 4) to regulate the relative temporal behavior of the flaps.

Figure 4 demonstrates how these gates perform specific logic operations. The exclusive OR (XOR) function is achieved by introducing either PNPP or H_2O_2 into the solution (see Fig. 4A). Only the set of flaps with the appropriate catalyst for the reaction will fold together; i.e., either the two yellow flaps (Fig. 4C) or the green flaps (Fig. 4D) will join together. When both H_2O_2 and PNPP are added to the solution, all four flaps come together (Fig. 4E) and serve as the AND operation (Fig. 4B). Last, when neither of the appropriate reactants are present, the flaps remain flat in their original configuration to signify the NOT operation. These basic functions can be combined to perform more complicated logic operations. In this manner, these elements form the rudimentary components of microfluidic devices that can perform different computational tasks.

Notably, a passive sheet (i.e., not coated with catalysts) in the reactant-filled chamber cannot achieve the dynamic behavior described above. The catalytic coating is necessary to generate the flows that bend the compliant layer and thus allow the active sheets to perform the specified functions (e.g., wrapping and flapping). To demonstrate other behaviors that are unique to the deformable, active sheets, we consider a rectangular elastic layer that is completely free to move in the fluid-filled chamber and describe illustrative examples where the sheet undergoes flow-driven shape changes to translate along the surface; i.e., it "morphs to move." These studies can provide guidelines for creating soft robotic objects that undergo both actuation and motion and thus aid in automating the performance of microfluidic devices.

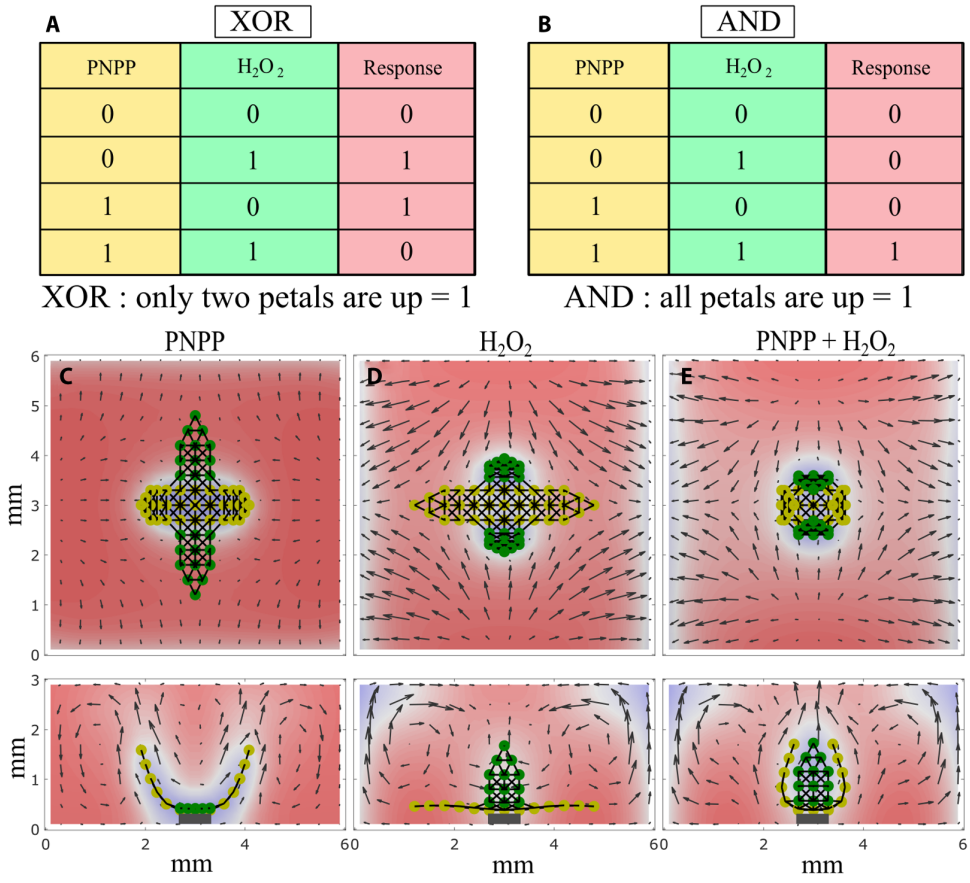

Fig. 4. Chemical logic gates, or flappers. Coating the petals with catalase (green) and AP (yellow) allows the system to perform different logic operations, such as XOR and AND [see corresponding truth tables (**A**) and (**B**)], as well as NOT. The XOR operation, defined when at least one of the opposing pair of petals is up, is achieved through introduction of either (**C**) PNPP or (**D**) H_2O_2 in the solution. (In this case, the "1" in the truth table indicates that two petals are bent upward.) (**E**) In the presence of both H_2O_2 and PNPP, all four flaps come together and serve as the AND operation. (In this case, "1" indicates that four petals are bent upward.) The corresponding reaction rates at the petals and on the walls for this simulation are set at $r^{cat}_{m,petal} = 2.67 \times 10^{-6} mol\,m^{-2}s^{-1}$, $r^{ap}_{m,petal} = 3.33 \times 10^{-7} mol\,m^{-2}s^{-1}$, $r^{cat}_{m,sidewall} = 4.5 \times 10^{-7} mol\,m^{-2}s^{-1}$, and $r^{ap}_{m,sidewall} = 6 \times 10^{-8} mol\,m^{-2}s^{-1}$. The NOT operation is achieved in the absence of both H_2O_2 and PNPP and is represented by all four flappers staying horizontally flat above the bottom surface.

For the cases below, our model incorporates the resistance associated with the sheet sliding against a surface. Specifically, we introduce a frictional force $\mathbf{f}_{fric} = -\gamma\langle\mathbf{v}\rangle$ that is proportional to the average velocity $\langle\mathbf{v}\rangle$ of the sheet nodes that lie within a specified cutoff distance from the bottom surface. Here, γ is a constant friction coefficient characterizing the interaction strength between the sheet and channel surfaces.

In the first example, we introduced small "bumps" that are modeled as sets of passive particles (gray spheres in Fig. 5) anchored at regular intervals on the bottom surface; the no-slip boundary conditions are imposed at these stationary bumps. At $t = 0$, we introduce an influx of H_2O_2 (for a specified amount of time) at the right end of the channel. When a noncoated, passive sheet is placed in this chamber and exposed to the influx, it is dragged by the flow to the left until it is arrested by the first bump and remains at the position despite the convective flow (Fig. 5A).

On the other hand, the flows generated by the catalase-coated sheet deform the active layer and give rise to the distinctive tumbling motion that allows the sheet to keep moving along the surface (Fig. 5, B to E). (To illustrate the sheet's motion, the following images are taken when the sample reaches the second bump shown in Fig. 5B.) As the sheet slides along the surface, its left end is temporarily arrested by the bump (Fig. 5C), while the right end is dragged up and forward by the flow from the right. Consequently, the right end of the sheet tumbles over the bump (Fig. 5D). The sheet is then flattened by the flow field and slides along the surface (Fig. 5E). Upon encountering the next bump, the leftmost beads will be arrested and the rightmost beads will tumble over the bump. With uniformly spaced bumps, this sliding and tumbling motion will continue until all the reactant is consumed.

The bumps in the simulations can represent small asperities or mounds of debris on the surface of the microchamber. If the sheet was used to transport cargo in the device, then the results in Fig. 5 indicate that the active layer could overcome small obstacles in its path and deliver the cargo to a desired location. The passive "transporter," however, becomes stuck at the first hurdle.

The second example of a morphing and moving sheet is inspired by the inchworm, which repeatedly bends and extends its body to achieve locomotion. To mimic this behavior, we use a catalase-coated sheet that is heavier at the front and back edges than the rest of the layer. (Similar results could be obtained by coating only the central portion of the layer with catalyst and the leaving the front and back edges uncoated, making these edges passive.) This sheet is placed on the

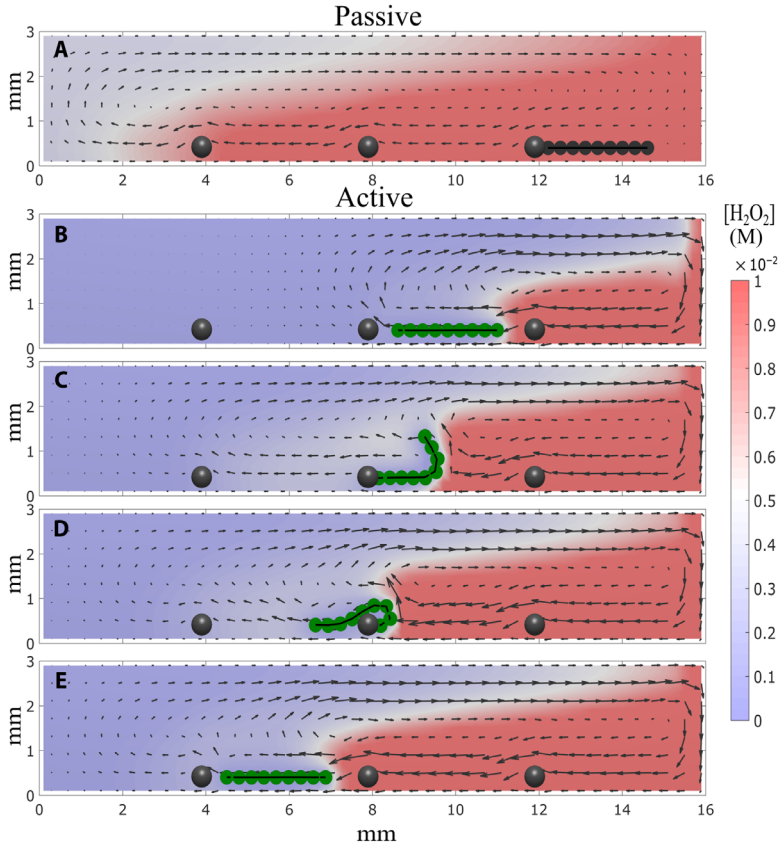

Fig. 5. Tumbling motion of active sheets. Motion of passive (**A**) and active (**B** to **E**) sheets on the bumpy surface due to an influx of H_2O_2 (with a rate $R = 4.5 \times 10^{-10}$ mol s^{-1}) through the right wall of the chamber. (A) The passive, noncoated sheet becomes arrested at the first bump. (B to E) Tumbling motion of the catalase-coated ($r^{cat}_{m,sheet} = 8.61 \times 10^{-3}$ mol m^{-2} s^{-1}) sheet. As the active sheet slides along the surface (B), the left end is temporarily arrested by the bump (C), while the right end is dragged upward by the flow due to the solutal force and pushed forward due to the influx of dense reactant. Consequently, the right end of the sheet tumbles over the bump (D). The sheet is then flattened by the flow field and slides along the surface to the next bump (E), at which point the process is repeated.

bottom wall at the right end of the chamber, which is initially devoid of reactants (H_2O_2) and then subjected to a sequential influx of H_2O_2, much as a car is sprayed by regularly spaced hoses as it moves through a car wash. An influx of H_2O_2 (over a specified time) is delivered from the right wall; next, reactant is released in a sequential manner from regularly spaced and oppositely placed sites on the two side walls (at $x = 16$ mm and $x = 23$ mm).

In the case of a completely passive sheet, the layer moves along the surface in a flat configuration, driven by the convective flows generated by the release of the heavy reactant into the aqueous solution (see Fig. 6A). On the other hand, the active sheet responds to each influx of H_2O_2 "fuel" by undergoing the distinctive motion seen in Fig. 6 (B to D). Recall that both sides of the active sample are coated with catalyst, and the sheet is kept close to the surface by gravity. With the first influx from the right, the sheet is propelled by the outward flow from the reactant-rich solution (marked in red). When some fraction of H_2O_2 diffuses to the bottom side of the sheet, it is converted into the lighter products, which flow upward. This upward flow pushes the central portion upward. Since the edges of the sheet are heavier than the rest, it is only this central area that is lifted by the upward flow. Consequently, the sheet assumes an inchworm-like position, with both "head" and "tail" at the surface (see inset in Fig. 6). Eventually, the greater upward and inward flow on the top side of the sample causes the sheet to flatten out (Fig. 6D).

Ultimately, the available reactant is consumed, and the flat, active sheet ceases to move. With the next influx of H_2O_2, however, some fraction of this reactant again interacts with the bottom of the sheet and the cycle of motion is repeated (Fig. 6, E and F), thereby allowing the sheet to effectively creep along the surface.

The examples in Figs. 5 and 6 provide elementary design rules for devising active, responsive sheets that undergo shape changes and locomotion. With additional patterning of the sheet, fluid flow, or surface, we anticipate that the range of "morph to move" maneuvers exhibited by the active sheet can be greatly expanded.

DISCUSSION

We have undertaken the first study of the response of a flexible, catalyst-coated sheet to self-generated flow fields, which arise from the catalytic reaction in the host solution. The findings from our computational models reveal how the coupling between these deformable, active sheets and the reactant-containing fluids leads to rich dynamic behavior, which extends the functionality and utility of active materials. Namely, a reconfigurable, self-propelled fabric can perform a wider range of tasks than an active hard particle. For instance, the four-petal sheet can act as a "hand" with controllable "fingers," which can act in concert (to enwrap objects) or sequentially (to perform logic operations). The functionality of the active sheets is not limited to these

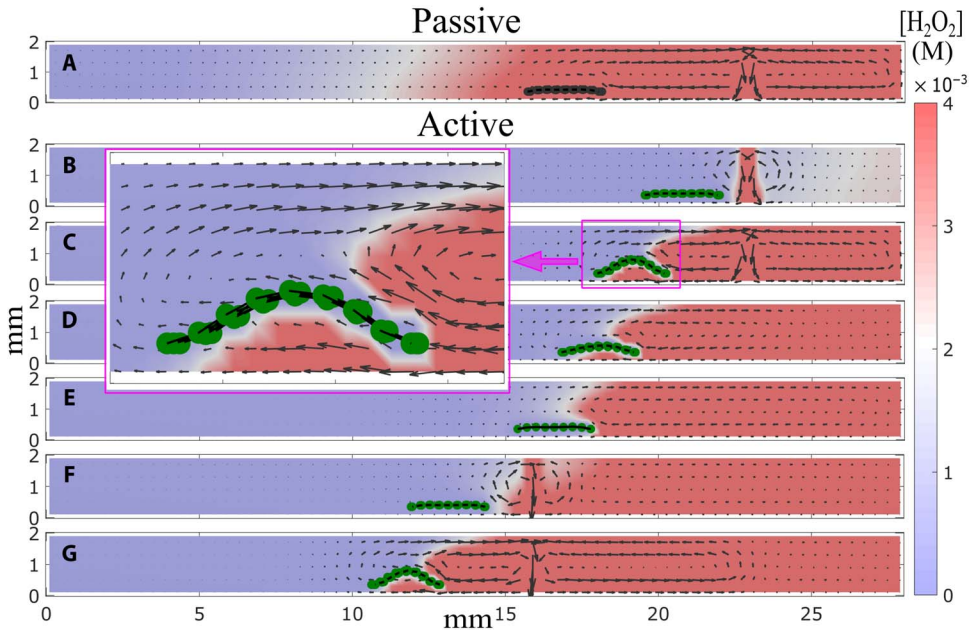

Fig. 6. Creeping motion of active sheets. Response of passive (**A**) and active (**B** to **G**) sheets to the sequential influxes of H_2O_2 (at a rate $R = 1.8 \times 10^{-9}$ mol s^{-1}). Initially, H_2O_2 is introduced at the right end; in subsequent cycles, it is injected from both side walls at regularly spaced positions in *x*. (A) The passive sheet simply slides along the surface as H_2O_2 is introduced into the chamber. (B to G) Inchworm-like motion of the catalase-coated, active sheet with a nonuniformly distributed mass. The sheet is lighter in the center and heavier at the left and right edges. With an influx of the dense, reactant-rich solution, the active sample moves away from the regions where H_2O_2 is introduced. Simultaneously, catalase on the sample ($r^{cat}_{m,sheet} = 8.61 \times 10^{-3}$ mol m^{-2} s^{-1}) decomposes H_2O_2 to less dense products, which flow upward. The lighter, central portion of the sheet is pushed upward by this flow, but the heavier edges (head and tail) remain on the bottom surface; inset in (C) shows a blowup of this configuration. As the reactant is depleted and reaction ceases to produce the less dense products, the sheet flattens out. This cycle of motion is repeated, with each influx of H_2O_2, thereby allowing the sheet to effectively creep along the surface.

illustrative examples. Moreover, various other catalytic reactions can be employed to promote the actuation and locomotion of the sample.

Here, we focused on catalytic reactions, where solutal buoyancy is the dominant mechanism for producing the fluid flow. Alternatively, diffusiophoretic mechanisms could be used to couple evolving chemical concentrations to generated fluid flows to move and shape flexible, active sheets. With diffusiophoretic mechanisms, however, the generated flows are driven at the fluid-solid interfaces, and the velocities of the flows (determined by interactions between the dissolved chemicals and the solid wall) are quite slow [~10 μm/s (*18*)]. In contrast, the effects due to solutal buoyancy scale with the cube of the characteristic length scale of the chamber and produce the maximum fluid velocities in the interior of the chamber (with zero velocities at the boundaries). Hence, the entire "interior region" of the flow field can be used to efficiently sculpt the shape of the flexible sheet and "mold" the dynamic behavior of the system. In addition, the fluid velocities can be adjusted (by altering the height of the chamber) to achieve speeds that are sufficient to operate sheets with the desired mode of functionality. Notably, the force produced from solutal buoyancy flows is sufficiently large to propel the collective behavior of isolated particles (*8*) and hence is adequate to transport the thin sheets considered here.

Through these studies, we isolated behavior that occurs when a chemical reaction cascade (where the product of one reaction is the reactant for the next) is coupled to deformable, chemically patterned sheets (as in Fig. 2). We demonstrated how to regulate the multiple temporal events occurring between the sheet and the solution-filled chamber by coating the walls of the container with specific surface concentrations of the appropriate catalyst. By tailoring these surface concentrations, we can adjust the rates of the reactions to introduce time delays between different dynamic elements in the system. Furthermore, with the coated sheets and walls, we can controllably orient the directionality of the flow throughout the chamber (as in Fig. 3) and thereby generate the necessary patterns in the fluids to tailor the sheet's shape and dynamic behavior.

The ability to introduce and control time delays, and thereby orchestrate the temporal responses of the different petals or flaps, provides a means of introducing new functionality into fluidic systems. For example, this delay can be used to regulate the motion of the particles along specific paths at specific time intervals, much like traffic lights regulate the movement of vehicles. This level of regulation is vital for creating stand-alone microfluidic devices that autonomously perform multistage chemical analyses or carry out separate, sequential steps to construct complex, three-dimensional structures from dispersed particles in the solution.

Last, the example of the deformable creeper in Fig. 6 allowed us to illustrate how spatial variations within a rectangular sheet are useful for achieving specified modes of bio-inspired movement. In particular, the spatial patterning allowed us to distinguish the "body" from the "feet" and precisely coordinate the dynamic behavior of each part. Our specific choice of spatial patterning allowed the body to bend upward, while the feet remained localized on the surface and thus form the distinctive shape that characterizes the locomotion of an inchworm. Determining approaches that drive soft, deformable materials to actuate and move in such a controlled manner is valuable for creating bio-inspired, small-scale robotic systems that can perform mechanical work.

Moving forward, these studies provide a foundation to address another intriguing scientific challenge: how to harness the catalytic reactions to alter not only the shape and motion of the sheets but also the

sheet's material properties. For example, for catalytic reactions that give rise to thermal buoyancy effects (*12*), the generated heat could be exploited to also modify the local swelling or modulus of a thermo-responsive gel film. Thus, with the appropriate combination of reactants, catalysts, and catalyst-coated, responsive materials, researchers could design self-propelled, shape-shifting sheets that autonomously modify their physical properties in response to the self-generated stimulus. Such design choices can facilitate the fabrication of autonomously functioning, self-regulating systems (*19*). In recent years, researchers have synthesized a range of stimuli-responsive gels (*9*, *20*–*23*) that undergo changes in mechanical behavior in response to different stimuli. Catalyst-coated gel sheets that produce the specific stimulus (e.g., heat or light) that alters their mechanical properties, as well as propels their motion and reconfiguration, would be highly useful for the next generation of autonomously performing soft-robotic materials systems.

METHODS

Equations 1 to 4, along with the corresponding boundary conditions (Eq. 5), were solved numerically using a combination of the lattice Boltzmann method (LBM) (*24*) for the fluid dynamics and the IB method for an elastic sheet (*14*, *25*). Within the IB model, which couples the sheet to the fluid, each node is represented by a particle with an effective hydrodynamic radius a that experiences fluid drag, characterized by the mobility $\mu = (6\pi\eta a)^{-1}$. In other words, the elastic sheet, represented by a single-layer network of the interconnected mesh nodes, has an effective thickness equal to the hydrodynamic radius a of a single node.

The forces exerted by the sheet on the fluid are included in $\mathbf{F}_{el}$ and were calculated using the IB approach (*14*, *25*). The implementation of the fluid-structure interaction via the IB method (*14*, *25*) provides zero fluid velocities at the discretization nodes of the structure (sphere or sheet in our case) and, therefore, approximates the no-slip condition for the fluid velocity at the boundary nodes, as well as no fluid permeation through the discretized boundaries of the immersed objects. [While we have chosen to use the IB in this implementation, there are various approaches to modeling fluid-structure interactions between mobile, elastic surfaces and the surrounding fluid; these approaches include the stochastic Eulerian Lagrangian method (*26*), the IB method with adaptive mesh refinement (*27*), and a coupling of the LBM to the lattice spring model (*28*).]

In the simulation scheme, at each time step, we first used a single-relaxation time LBM to solve the continuity (Eq. 1) and Navier-Stokes (Eq. 2) equations and thereby obtained the velocity field $\mathbf{u} = (u_x, u_y, u_z)$ and pressure field p. Then, a second-order finite difference scheme was used to solve the diffusion terms in Eq. 3. The computed flow field $\mathbf{u}$ was used to advect the chemical concentration (Eq. 3) and to update the location of the mesh points (particles) of the suspended sheet (Eq. 4). The updated concentration field, C_i, was then used to model further consumption near the catalytic nodes. This procedure was repeated over 12×10^6 iterations to simulate physical times that correspond to values between 6 and 24 hours (i.e., the time scale for the corresponding experimental observations).

The size of the fluid-filled chamber is $L_x \times L_y \times L_z = 30$ by 30 by 15 in lattice Boltzmann units (Δx). To maximize the effects responsible for interactions of the flow in the channel with the structure of the chemically active sheet, we used two sets of LBM discretization with grid spacings $\Delta x_1 = 100\mu m$ and $\Delta x_2 = 200\mu m$. These sets of parameters yield channels with physical dimensions equal to 3 mm by 3 mm by 1.5 mm and 6 mm by 6 mm by 3 mm, respectively. In the discretization of the elastic sheet, the separation between two nearest neighboring nodes was set to $1.5\Delta x$. Hence, the dimensions of the sheet for two cases are $l = 3$ mm and $l = 6$ mm, respectively, in length, and their thicknesses (determined by the effective hydrodynamic diameters of the constituent nodes) are approximately $d = 0.26$ mm and $d = 0.52$ mm, respectively.

SUPPLEMENTARY MATERIALS

Supplementary material for this article is available at http://advances.sciencemag.org/cgi/content/full/4/12/eaav1745/DC1

Movie S1. Wrapping and unwrapping of a catalase-coated flower-like sheet around a capsule.

Movie S2. Periodic wrapping and unwrapping of a catalase-coated flower-like sheet around a capsule.

Movie S3. Temporal delay in bending of catalase-coated green and GOx-coated pink petals of the flower.

Movie S4. Crawling motion of a catalase-coated rectangular sheet over a bumpy terrain.

Movie S5. Creeping motion of a catalase-coated rectangular sheet over the bottom surface of the channel.

REFERENCES AND NOTES

1. S. J. Ebbens, Active colloids: Progress and challenges towards realising autonomous applications. *Curr. Opin. Colloid Interface Sci.* **21**, 14–23 (2016).
2. X. Ma, A. C. Hortelão, T. Patiño, S. Sánchez, Enzyme catalysis to power micro/nanomachines. *ACS Nano* **10**, 9111–9122 (2016).
3. S. Sengupta, D. Patra, I. Ortiz-Rivera, A. Agrawal, S. Shklyaev, K. K. Dey, U. Córdova-Figueroa, T. E. Mallouk, A. Sen, Self-powered enzyme micropumps. *Nat. Chem.* **6**, 415–422 (2014).
4. S. Das, A. Garg, A. I. Campbell, J. Howse, A. Sen, D. Velegol, R. Golestanian, S. J. Ebbens, Boundaries can steer active Janus spheres. *Nat. Commun.* **6**, 8999 (2015).
5. J. Li, O. E. Shklyaev, T. Li, W. Liu, H. Shum, I. Rozen, A. C. Balazs, J. Wang, Self-propelled nanomotors autonomously seek and repair cracks. *Nano Lett.* **15**, 7077–7085 (2015).
6. L. Baraban, M. Tasinkevych, M. N. Popescu, S. Sanchez, S. Dietrich, O. G. Schmidt, Transport of cargo by catalytic Janus micro-motors. *Soft Matter* **8**, 48–52 (2012).
7. D. Patra, S. Sengupta, W. Duan, H. Zhang, R. Pavlick, A. Sen, Intelligent, self-powered, drug delivery systems. *Nanoscale* **5**, 1273–1283 (2013).
8. O. E. Shklyaev, H. Shum, V. V. Yashin, A. C. Balazs, Convective self-sustained motion in mixtures of chemically active and passive particles. *Langmuir* **33**, 7873–7880 (2017).
9. B. E. Treml, R. N. McKenzie, P. Buskohl, D. Wang, M. Kuhn, L.-S. Tan, R. A. Vaia, Autonomous motility of polymer films. *Adv. Mater.* **30**, 1705616 (2018).
10. H. S. Kim, C. H. Lee, P. K. Sudeep, T. Emrick, A. J. Crosby, Nanoparticle stripes, grids, and ribbons produced by flow coating. *Adv. Mater.* **22**, 4600–4604 (2010).
11. I. Ortiz-Rivera, H. Shum, A. Agrawal, A. Sen, A. C. Balazs, Convective flow reversal in self-powered enzyme micropumps. *Proc. Natl. Acad. Sci. U.S.A.* **113**, 2585–2590 (2016).
12. L. Valdez, H. Shum, I. Ortiz-Rivera, A. C. Balazs, A. Sen, Solutal and thermal buoyancy effects in self-powered phosphatase micropumps. *Soft Matter* **13**, 2800–2807 (2017).
13. S. Chandrasekhar, *Hydrodynamic and Hydromagnetic Stability* (Clarendon Press, 1961).
14. S. Lim, A. Ferent, X. S. Wang, C. S. Peskin, Dynamics of a closed rod with twist and bend in fluid. *SIAM J. Sci. Comput.* **31**, 273–302 (2008).
15. J. Switala, P. C. Loewen, Diversity of properties among catalases. *Arch. Biochem. Biophys.* **401**, 145–154 (2002).
16. G. Gaetani, A. M. Ferraris, M. Rolfo, R. Mangerini, S. Arena, H. N. Kirkman, Predominant role of catalase in the disposal of hydrogen peroxide within human erythrocytes. *Blood* **87**, 1595–1599 (1996).
17. J. Raba, H. A. Mottola, Glucose oxidase as an analytical reagent. *Crit. Rev. Anal. Chem.* **25**, 1–42 (1995).
18. J. L. Anderson, Colloid transport by interfacial forces. *Annu. Rev. Fluid Mech.* **21**, 61–99 (1989).
19. X. He, M. Aizenberg, O. Kuksenok, L. D. Zarzar, A. Shastri, A. C. Balazs, J. Aizenberg, Synthetic homeostatic materials with chemo-mechano-chemical self-regulation. *Nature* **487**, 214–218 (2012).
20. A. S. Gladman, E. A. Matsumoto, R. G. Nuzzo, L. Mahadevan, J. A. Lewis, Biomimetic 4D printing. *Nat. Mater.* **15**, 413–418 (2016).
21. O. Kuksenok, A. C. Balazs, Modeling the photoinduced reconfiguration and directed motion of polymer gels. *Adv. Funct. Mater.* **23**, 4601–4610 (2013).

22. S.-J. Jeon, A. W. Hauser, R. C. Hayward, Shape-morphing materials from stimuli-responsive hydrogel hybrids. *Acc. Chem. Res.* **50**, 161–169 (2017).
23. M. A. C. Stuart, W. T. S. Huck, J. Genzer, M. Müller, C. Ober, M. Stamm, G. B. Sukhorukov, I. Szleifer, V. V. Tsukruk, M. Urban, F. Winnik, S. Zauscher, I. Luzinov, S. Minko, Emerging applications of stimuli-responsive polymer materials. *Nat. Mater.* **9**, 101–113 (2010).
24. Z. Guo, C. Zheng, B. Shi, Discrete lattice effects on the forcing term in the lattice Boltzmann method. *Phys. Rev. E* **65**, 046308 (2002).
25. H. Shum, A. Tripathi, J. M. Yeomans, A. C. Balazs, Active ciliated surfaces expel model swimmers. *Langmuir* **29**, 12770–12776 (2013).
26. P. Plunkett, J. Hu, C. Siefert, P. J. Atzberger, Spatially adaptive stochastic methods for fluid–structure interactions subject to thermal fluctuations in domains with complex geometries. *J. Comput. Phys.* **277**, 121–137 (2014).
27. B. E. Griffith, R. D. Hornung, D. M. McQueen, C. S. Peskin, An adaptive, formally second order accurate version of the immersed boundary method. *J. Comput. Phys.* **223**, 10–49 (2007).
28. A. Alexeev, R. Verberg, A. C. Balazs, Designing compliant substrates to regulate the motion of vesicles. *Phys. Rev. Lett.* **96**, 148103 (2006).

Acknowledgments: We acknowledge helpful conversations with Prof. Jennifer Ross. **Funding:** A.C.B. gratefully acknowledges funding from NSF grant 1740630: CCI Phase I: Center for Chemomechanical Assembly and the computational facilities at the Center for Research Computing at the University of Pittsburgh. **Competing interests:** The authors declare that they have no competing interests. **Author contributions:** All authors designed the system described here and determined the studies to be performed. A.L. and O.E.S. performed the simulations. All the authors helped analyze the data and contributed to writing the manuscript. **Data and materials availability:** All data needed to evaluate the conclusions in the paper are present in the paper and/or the Supplementary Materials. Additional data related to this paper may be requested from the authors.

Submitted 21 August 2018
Accepted 20 November 2018
Published 21 December 2018
10.1126/sciadv.aav1745

Citation: A. Laskar, O. E. Shklyaev, A. C. Balazs, Designing self-propelled, chemically active sheets: Wrappers, flappers, and creepers. *Sci. Adv.* **4**, eaav1745 (2018).

Designing self-propelled, chemically active sheets: Wrappers, flappers, and creepers

Abhrajit Laskar, Oleg E. Shklyaev and Anna C. Balazs

Sci Adv **4** (12), eaav1745.
DOI: 10.1126/sciadv.aav1745